Dissolution of realgar by *Acidithiobacillus ferrooxidans* in the presence and absence of zerovalent iron: Implications for remediation of iron-deficient realgar tailings

Lijun Fan[1], Fenghua Zhao[1], Jing Liu[2, ^], Karen A. Hudson-Edwards[3, *]

[1] College of Geoscience and Surveying Engineering, China University of Mining & Technology, Beijing 100083, China.

[2] The Key Laboratory of Solid Waste Treatment and Resource, Ministry of Education, Southwest University of Science and Technology, 621010 Mianyang China. ^ Corresponding author liujing-vip@163.com

[3] Environment & Sustainability Institute and Camborne School of Mines, University of Exeter, Penryn, Cornwall TR10 9DF, UK. * Corresponding author. Email: k.hudson-edwards@exeter.ac.uk; Tel: +44(0)1326-259489.

Date of re-submission: Accepted version 31 May 2018

Chemosphere code: CHEM21524

Keywords: realgar; ZVI; *A. ferrooxidans*; dissolution; arsenic.

Abstract

Realgar (As_4S_4)-rich tailings are iron-deficient arsenical mine wastes. The mechanisms and products of the dissolution of realgar by *Acidithiobacillus ferrooxidans* (*A. ferrooxidans*) in the presence (0.2 g and 2 g) and absence of zerovalent iron (ZVI) are investigated for three stages (each of 7 d with fresh *A. ferrooxidans* medium addition between the stages). SEM-EDX, FTIR, XPS and selective extraction analysis are used to characterize the solid-phase during the experiments. ZVI addition causes the systems to become more acid-generating, although pH increases are observed in the first day due to ZVI dissolution. Arsenic is released to solution due to realgar oxidation (~30 mg L^{-1} in the 0 g ZVI system in Stage I), but low concentrations are observed in the ZVI-added systems (<5 mg L^{-1}) and in Stages II and III of the 0 g ZVI system. As(III) dominates the released As(T) at day 1 (83-89% of As(T)), but is largely oxidized to As(V) at day 7 of each stage (53-98% of As(T)). Arsenic attenuation is attributed to the formation of mixed As-Fe oxyhydroxides and oxyhydroxy sulfates that take up released arsenic and are abundant in the 2.0 g ZVI system, and to passivation of the realgar surface. Consequently, a new strategy that combines *A. ferrooxidans* and exogenous ZVI addition for treating *in-situ* iron-deficient realgar-rich tailings is proposed, although its long-term effects need to be monitored.

1. Introduction

Arsenic (As) is a ubiquitous concern worldwide because of its toxic, carcinogenic and teratogenic properties on human health (Smith et al., 1992; Nordstrom and Alpers, 1999; Smedley and Kinniburgh, 2002). Dissolution of As-rich tailings is one of main causes of As contamination in water, soil and diverse ecosystems (Macur et al., 2001; Mkandawire and Dudel, 2005; Shi et al., 2017). The behavior of As in tailings and soils is strongly influenced by the oxidative and reductive microbial dissolution of As-bearing sulfides and Fe oxyhydroxides (Johnston et al., 2011; Lu and Wang, 2012; Burton et al., 2013). Arsenopyrite (FeAsS) and arsenian pyrite ($Fe(S, As)_2$) are common iron-rich As sulfides that can incorporate gold, silver, *etc.*, but mining and hydrometallurgy operations involving them can result in significant release of As to the environment (Reich et al., 2005; Corkhill and Vaughan, 2009). Microbial techniques can be used to treat these mine wastes by enhancing As immobilization (Gonzalezcontreras et al., 2010, 2012; Okibe et al., 2017). For example, Egal et al. (2009) found that various *Acidithiobacillus ferrooxidans* (*A. ferrooxidans*) strains can help the formation of kinds of ferric oxyhydroxy sulfates (*e.g.* tooeleite, schwertmannite and jarosite) that are able to incorporate As within their structure or adsorb them at their surface during microbial Fe(II) oxidation. Gonzalezcontreras et al. (2010) have shown that *Acidianus sulfidivorans* can promote the formation of scorodite ($FeAsO_4 \cdot 2H_2O$), which has low solubility and is a good mineral trap for As.

Arsenian pyrite can contain up to 10 wt.% As (Qiu et al., 2017). The microbial dissolution of pyrite involving organisms such as *A. ferrooxidans* has been studied for more than forty years (Singer and Stumm, 1970; Percak-Dennett et al., 2017). *A. ferrooxidans* is an acidophilic iron-oxidizing bacteria which oxidizes Fe(II) to Fe(III) at pH 1.5-7.0 to obtain energy for growth (Meruane and Vargas, 2003; Ko et al., 2013). The released Fe(III) can also oxidize pyrite and increase its dissolution rate. The oxidative dissolution of arsenopyrite, leading to the release of As(III) and As(V), has also

been extensively studied (Barrett et al., 1993; Corkhill and Vaughan, 2009). It has been shown that addition of excess Fe(III) can trigger electron transfer between Fe(III) and Fe(II) in arsenian pyrite and arsenopyrite dissolution, resulting in higher oxidative dissolution rates and production of secondary phases such as iron oxyhydroxides (Chen et al., 2014; Neil and Jun, 2016). These newly-formed iron oxyhydroxides can in turn sequester As via sorption or co-precipitation reactions (Dixit and Hering, 2003; Root et al., 2009; Johnston et al., 2012).

Realgar (As_4S_4) is another common As sulfide (containing mainly As(II)) (Lengke and Tempel, 2003; Wu et al., 2017), but compared to arsenopyrite and pyrite, is iron-deficient. Like the other As-bearing sulfides, realgar dissolution can be affected by physical, chemical and biological factors including pH, Eh, oxygen, light, solution composition/speciation and microorganism activity (Cullen and Reimer, 1989; Kyono et al., 2005). *A. ferrooxidans*, for example, has been shown to oxidize realgar (Zhang et al., 2007; Chen et al., 2011; Yan et al., 2017). Zhang et al. (2007) showed that the oxidation of realgar in acidic condition was significantly accelerated in the presence of dissolved Fe(II) and mixed cultures of *A. ferrooxidans* and *A. thiooxidans*, compared to single culture experiments. By contrast, Chen et al. (2011) found that microbially-generated Fe(III) can prevent the oxidation of realgar. These studies have mainly focused on the effects of aqueous iron ions (*e.g.* Fe(II), Fe(III)) and no studies to date have been carried out to investigate the effect of exogenous solid zerovalent iron (ZVI) on the dissolution of realgar. ZVI is a wide and effective commercial remediation agent used to remove As and other contaminants from groundwater and soils (Kuijae et al., 2009; Tuček et al., 2017; Xie et al., 2017). Recently, Liang et al. (2017) used ZVI to stabilize As-containing sludge, and showed that the extent of ZVI oxidation was closely related to its As sorption capacity. These findings raise important questions. What will happen when ZVI is added to iron-deficient As sulfides such as realgar? What are the mechanisms of As release during microbial realgar

dissolution with and without ZVI? An understanding of the mechanisms and products of realgar dissolution by *A. ferrooxidans* with ZVI would answer these questions. If the process is effective, exogenous ZVI combined with *A. ferrooxidans* might be an efficient remediation strategy for *in-situ* realgar-containing tailings.

Therefore, the aim of this study was to determine the mechanisms and products of realgar dissolution by *A. ferrooxidans* with and without ZVI. We used *A. ferrooxidans* since it is a common bacterium in AMD system and it is tolerant to, but does not metabolize, As (Jones et al., 2003; Yan et al., 2017). The specific objectives of the study were to (i) investigate the behavior and speciation of As during realgar dissolution; (ii) determine the character and stability of the secondary products; (iii) identify the mechanisms involved. This knowledge will be beneficial for developing remediation schemes for *in-situ* iron-deficient realgar-rich tailings.

2. Materials and methods

2.1. Sample preparation

The raw realgar used in this study was obtained from the Shimen Realgar Mine (Hunan Province, China), the largest former As supplier in Asia (Chen et al., 2017; Fan et al., 2018). The realgar was ground, sieved to less than 100 mesh (<180 μm) and without any other treatment to represent typical realgar tailings. X-ray diffraction (XRD) analysis confirmed that realgar was the dominant phase with no distinct diffraction peaks of other minerals observed (Fig. S1). X-ray fluorescence (XRF) analysis showed that the realgar was composed mainly of As (63 wt.%), S (3.46 wt.%) and Fe (4.5 wt.%), with minor amounts of Si (0.36 wt.%), Ca (0.26 wt.%), Al (0.26 wt.%), Sb (0.01 wt.%) and Se (0.06 wt.%). The ZVI powder used in the experiments was purchased from Sinopharm Chemical Reagent Co., Ltd (China), and XRD analysis showed it was composed of pure iron (Fig. S2). All chemicals

and reagents used in this study were of analytical grade and all solutions were prepared with deionized water (Milli-Q, Millipore, ≥18.2 MΩ cm).

2.2. Bacterial strain and bioleaching procedure

The *A. ferrooxidans* strain (*Acidithiobacillus ferrooxidans* SW 02) used in this study was provided by the Key Laboratory of Solid Waste Treatment and Resource Recycle, Southwest University of Science and Technology, Mianyang, China. Pure cultures of *A. ferrooxidans* cells were incubated at 30 °C in 9K liquid medium as follows: 1 L media of 0.5 g $K_2HPO_4 \cdot 3H_2O$, 0.01 g $CaNO_3$, 0.1 g KCl, 0.5 g $MgSO_4 \cdot 7H_2O$, 3 g $(NH_4)_2SO_4$, 44.3 g $FeSO_4 \cdot 7H_2O$, pH 2.2 (adjusted with 5 M H_2SO_4) (Silverman and Lundgren, 1959). Cells were harvested during the late exponential growth phase.

Batch experiments were carried out in 250 mL Erlenmeyer flasks under ambient air on a rotary shaker at 150 rpm and 30 °C for three stages (7 d per stage), which are hereafter denoted as Stage I, II and III. The flasks were covered loosely with nonwoven cloth to decrease water evaporation. Microcosms were designed using 100 mL *A. ferrooxidans* culture mixed with 1 g ground realgar at a pulp density of 1 % (w/v). Triplicate realgar microcosms were employed for each mass of ZVI added (0 g, 0.2 g, 2.0 g). The control treatment was set as 1 g realgar in 100 mL sterilized *A. ferrooxidans* liquid medium without ZVI addition. The medium in the Erlenmeyer flasks was replaced with 100 mL fresh *A. ferrooxidans* culture every 7 d (one stage) to ensure adequate bacteria activity. At regular intervals, *ca.* 5 mL aliquots were withdrawn using a pipette and immediately passed through a 0.22 μm cellulose membrane filter and acidified (10% HCl) for the total As and Fe (As(T) and Fe(T)) analysis. The extracted aliquots were compensated by the addition of 5 mL sterilized 9K medium. The solid samples were separated from the supernatant by vacuum filtration (SHB-IIIG, China), washed three times with de-ionized water and freeze-dried (Labonco, FreeZone, USA) for

characterization.

2.3. Aqueous-phase analysis

The pH and Eh were measured using a freshly calibrated pH meter (Sartorius PB-21) and HACH440d meter with a platinum electrode (MTC 10103). Aqueous Fe(T) and As(T) concentrations were determined by Inductive Coupled Plasma Emission Spectrometry (ICP-AES, iCAP6500 Thermo Fisher, USA). For concentrations below the ICP-AES detection limit (0.08 mg L^{-1}), As concentrations were determined using Inductively Coupled Plasma Mass Spectrometry (ICP-MS, Agilent 7700, USA). Concentrations of As(V) and As(III) were quantified by high-performance liquid chromatography (HPLC, SAP-20, Jitian, China) with a Hamilton PRP-X100 ion exclusion column linked to an atomic fluorescence spectrometer (AFS-8230, Jitian, China), with a detection limit of 0.01 μg L^{-1}. Aqueous As speciation was measured at day 1 and 7 of each stage due to the growth cycle of *A. ferrooxidans*. The relative error of As(T) measured by ICP-AES/ICP-MS and HPLC-AFS (calculated by the sum of As(III) and As(V)) was less than 1.5%.

2.4. Solid-phase Characterization

X-ray diffraction (XRD) patterns of raw realgar and ZVI powder were recorded using an X' Pert PRO (PANalytical, Netherland) instrument with a Cu-Kα source. Diffraction data were acquired over a 2θ range of 10-90 ° with a scan time of 10.16 s per step and a step size of 0.03 °. The bulk elemental compositions of powder sample were determined by X-ray fluorescence (XRF) analysis using a PANalytical Axios instrument equipped with a rhodium anode.

Changes in mineralogy were examined by Fourier Transform Infrared spectrometry (FTIR, Spectrum, Perkin Elmer) coupled with a diamond attenuated total reflection (ATR) in a spectral band

ranging from 400 cm^{-1} to 4000 cm^{-1} with a resolution of 1 cm^{-1} and 64 scans per sample. The surface morphology of the solid sample was imaged using Scanning Electron Microscopy (SEM, EVO@18, ZEISS) equipped with energy-dispersive-X-ray-spectroscopy (EDX) operating at 15 kV. Changes in solid-phase As, Fe and S oxidation states were determined by X-ray photoelectron spectroscopy (XPS, R3000, VG-Scienta) equipped with a Al-Kα source at 30 eV and a step size to 0.05 eV. The specimen surface was analyzed under an Ar^{+} beam in the vacuum chamber. Photoelectron binding energies were referenced to C1s level at 284.8 eV. The deconvolution of the raw data was fitted using the software of CasaXPS, and the Shirley-type background was subtracted before deconvolution and fitting. The binding energies for the component peaks of As, Fe, S were identified by comparison to previously reported values (Nesbitt and Muir, 1998; Ouyang et al., 2014).

Solid-phase samples retrieved from batch microcosms were also assessed using selective chemical extraction. Three fractions were extracted *i.e.* surface-adsorbed fraction (F1); the amorphous Fe (oxyhydr)oxides fraction (F2); crystallized Fe (oxyhydr)oxides fraction (F3) (Wenzel et al., 2001). Briefly, 0.25 g freeze-dried solid materials were weighed into 50-mL polypropylene centrifuge tubes in triplicate and selectively extracted using the reagents and methods listed in Table S1. After each extraction step, the suspensions were collected by centrifugation for 10 min at 10000 rpm. The extracts were filtered (0.22 μm) for As concentration analysis by ICP-AES.

3. Results and discussion

3.1 Dynamics of As and Fe release during realgar dissolution with and without ZVI

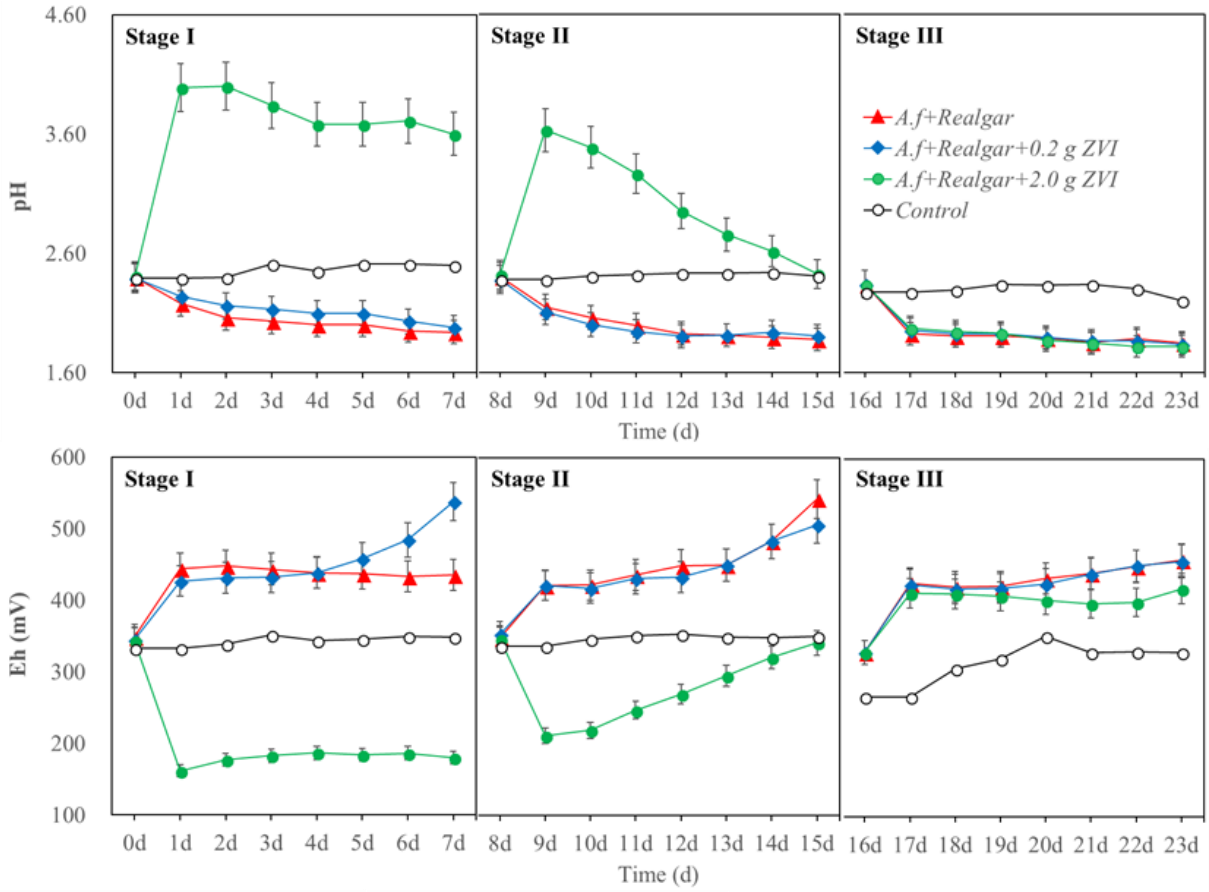

Fig. 1 Changes in pH and Eh during realgar dissolution by *A. ferrooxidans* with and without ZVI. The experiments were carried out over three stages (hereafter denoted as Stage I, II, III, 7 d per stage), with fresh *A. ferrooxidans* culture refreshment between Stages. Error bars denoted as standard deviations (n = 3).

pH and Eh variations are important indices for understanding mineral dissolution mechanisms in environmental systems (Burlo et al., 1999; Yamaguchi et al., 2011). Changes in pH and Eh as a function of time and ZVI presence and absence are shown in Fig. 1. The pH and Eh values in the control at every stage were relatively stable at ~2.4 and ~250-350 mV, respectively. In Stages I and II, dramatic increases in pH to ~3.5-4.0 and Eh decreases to ~180 mV were observed in the first day of the 2.0 g ZVI addition experiments. In Stage III, the 2.0 g ZVI experiment pH and Eh values were almost same as in the 0 g and 0.2 g ZVI experiments. The pH continuously decreased with corresponding increases in Eh in the 0 g, 0.2 g and 2.0 g ZVI experiments. High ZVI (2.0 g) addition

had the most significant influence on solution pH and Eh.

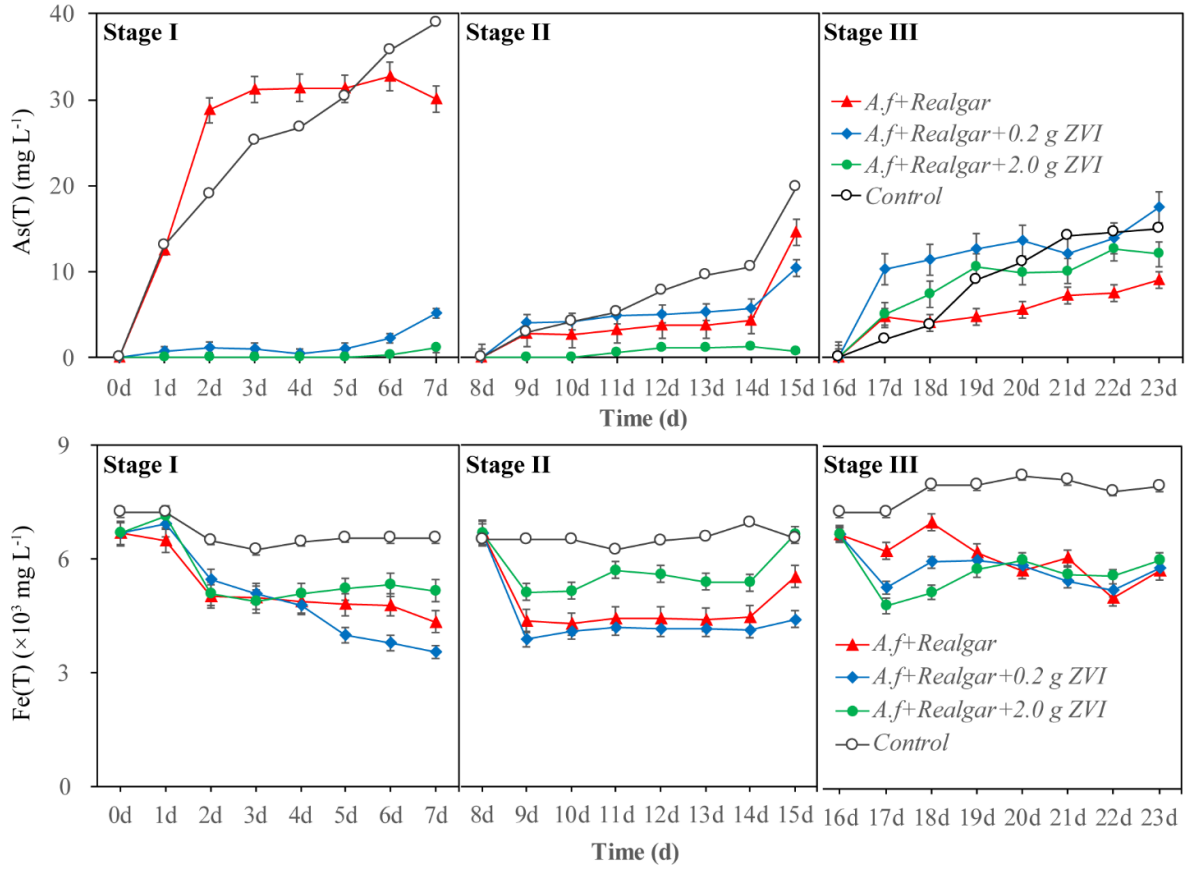

Fig. 2 Changes in aqueous As(T) and Fe(T) concentrations during realgar dissolution by *A. ferrooxidans* with and without ZVI. The experiments were carried out over three stages (hereafter donated as Stage I, II, III, 7 d per stage), with fresh *A. ferrooxidans* culture refreshment between Stages. Error bars denoted as standard deviations (n = 3).

Fig. 2 shows As(T) and Fe(T) leachate concentrations over the three stages. In Stage I, the As(T) release for the 0 g ZVI experiment rose dramatically to ~30 mg L^{-1} in the first two days, and the rate and extent of realgar dissolution was enhanced in the presence of *A. ferrooxidans* compared to the control (~20 mg L^{-1}). In Stage II As(T) release for the 0 g ZVI experiment plateaued, suggesting that dissolution reached steady-state, while in the control experiment As(T) increased to ~40 mg L^{-1}, eventually exceeding all of the other experiments. After fresh microbial culture addition between the two stages, As(T) concentrations for the 0 g ZVI experiment in Stages II and III were significantly less than those in Stage I, eventually rising to ~14.6 mg L^{-1} and ~9.1 mg L^{-1}, respectively.

Overall, the As(T) concentration patterns for the 0.2 g and 2.0 g ZVI experiments were similar throughout the experiment, but the magnitudes were dissimilar. In Stage I, As(T) concentrations were very low (<1 mg L^{-1}), but rose to *ca.* 5 mg L^{-1} at day 7, with those of the 0.2 g ZVI experiments slightly exceeding those of the 2.0 g ZVI experiments. As(T) concentrations were still low (<1 mg L^{-1}) in the 2.0 g ZVI experiments in Stage II, and were lower overall than those of 0.2 g ZVI experiments. In the latter, As(T) concentrations during the initial six days in Stage II were similar to those of day 7 in Stage I, but rose significantly to *ca.* 10 mg L^{-1} at day 15. As(T) concentrations in the 0.2 g ZVI Stage II experiment were higher than those of the 0 g ZVI experiment, except for day 7. In Stage III, As(T) concentrations for the 0.2 g and 2.0 g ZVI experiments were higher than those of the 0 g ZVI experiment. Concentrations rose during Stage III, and were highest for the 0.2 g ZVI experiment. In the control system, As(T) was highest at the end of each stage. The As(T) release rate in the first two days was slow, but then surpassed those of the ZVI and *A. ferrooxidans* addition experiments.

Fe(T) concentrations in the 0 g, 0.2 g and 2.0 g ZVI-added experiments were below those in the control treatment over the three stages. In Stage I, the concentration patterns of Fe(T) contrasted with those of As(T), and the Fe(T) concentrations declined through this stage (Fig. 2). Surprisingly, concentrations of Fe(T) were high (6400 mg L^{-1}) in the 0 g ZVI experiment, despite the fact that only realgar was used which had low amounts of Fe (4.5 wt.%). These high Fe(T) concentrations are ascribed to the $FeSO_4 \cdot 7H_2O$ used in the bacterial medium. Fe(T) concentrations in the 0 g, 0.2 g and 2.0 g ZVI experiments were clearly below the control experiment, and at the beginning of Stage I, were higher than those of 0 g ZVI experiment, suggesting that some iron was released through ZVI dissolution. After 4 d, Fe(T) concentrations in the 2.0 g ZVI experiment were still higher than those of 0 g ZVI experiment, suggesting that Fe was still released by ZVI dissolution. The opposite trend was observed in 0.2 g ZVI experiment, as concentrations fell below those of the 0 g ZVI, suggesting

that the Fe released by ZVI dissolution earlier in Stage I had been consumed.

In Stage II, Fe(T) concentrations were highest for the 2.0 g ZVI experiment, followed by the 0 g and 0.2 g ZVI experiments. In each experiment, Fe(T) concentrations were relatively stable until 15 d when they rose. In Stage III, Fe(T) concentrations were similar for the 0.2 g and 2.0 g ZVI experiments; they rose from 15 d to 19 d, declined slightly to 22 d, then rose slightly at 23 d. Fe(T) concentrations in the 0 g ZVI experiment were higher than those in the 0.2 g and 2.0 g ZVI experiments at 17 d of Stage III, but after peaking at 18 d, declined overall by 23 d to fall below those of 0.2 g and 2.0 g ZVI experiments.

3.2 Dynamic of aqueous As speciation changes during realgar dissolution with and without ZVI

Changes in aqueous As speciation during the experiments are shown in Fig. 3 and the data are compiled in Tables S4 and S5. The speciation of As in the control and in the 0 g, 0.2 g and 2.0 g ZVI-experiments were completely different. In the control experiment, the released As was dominantly As(III) (83-100% of As(T)) with only minor As(V) detected in these three stages. For the 0 g ZVI experiment in Stage I, the As(V) release rate was higher than that of As(III) (267 μg L^{-1} d^{-1} *vs.* 21 μg L^{-1} d^{-1}), while in Stages II and III, the release of As(III) decreased. The relative proportions of As(V) were 62%, 89% and 88% in Stage I of the 0 g, 0.2 g and 2.0 g experiments, respectively.

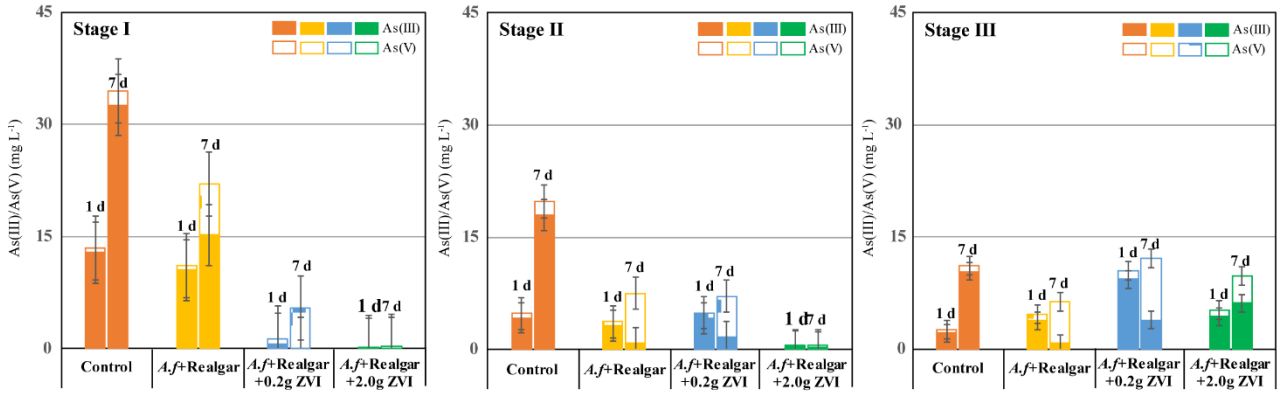

Fig. 3 Changes in aqueous As speciation during realgar dissolution by *A. ferrooxidans* with and without ZVI. The experiments were carried out at 1 d and 7d of each stage (three stages hereafter donated as Stage I, II, III), with

microbial culture refreshment between stages. Error bars denoted as standard deviations (n = 3).

Addition of 0.2 g ZVI decreased the proportion of As(III) and increased the proportion of As(V) (Fig. 3A-C). As(III) dominated at 1 d (83-89% of As(T)), whereas As(V) dominated at 7 d of each stage (66-98% of As(T)). As(III) also dominated at 1 d of the 2.0 g ZVI experiments. In contrast to the 0.2 g ZVI experiments, however, a relatively large proportion of As(III) was seen at 7 d of Stages II and III (37-47% of As(T)) in the 2.0 g ZVI experiments.

3.3 Formation of secondary products as a result of realgar dissolution with and without ZVI

Visible color changes were observed in the experiment process and the solid samples (Fig. 4 and Fig. S3). The color changed from red to brown with the increase of ZVI, indicating the variation of secondary mineral composition due to ZVI addition.

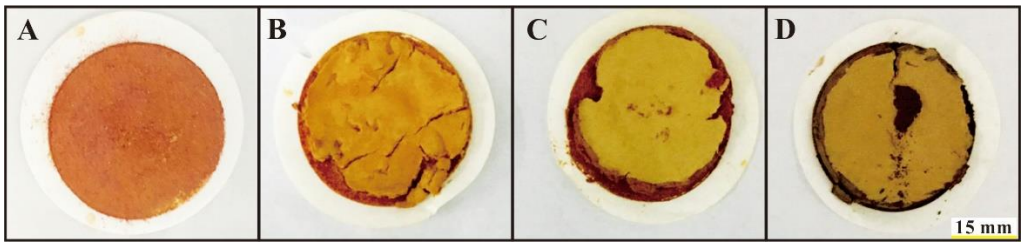

Fig. 4 Visible changes in color during realgar dissolution by *A. ferrooxidans* in three ZVI treatments after stage III. (A: control, B: 0 g ZVI, C: 0.2 g ZVI; 2.0 g ZVI).

In agreement with the color changes, SEM-EDX observations (Fig. 5) of the solid precipitates after the 2.0 g ZVI addition confirmed the presence of mixed Fe-O-As oxyhydroxides and hydroxy sulfates on the realgar surfaces. However, in the 0 g and 0.2 g ZVI systems, no As-bearing Fe precipitates were observed.

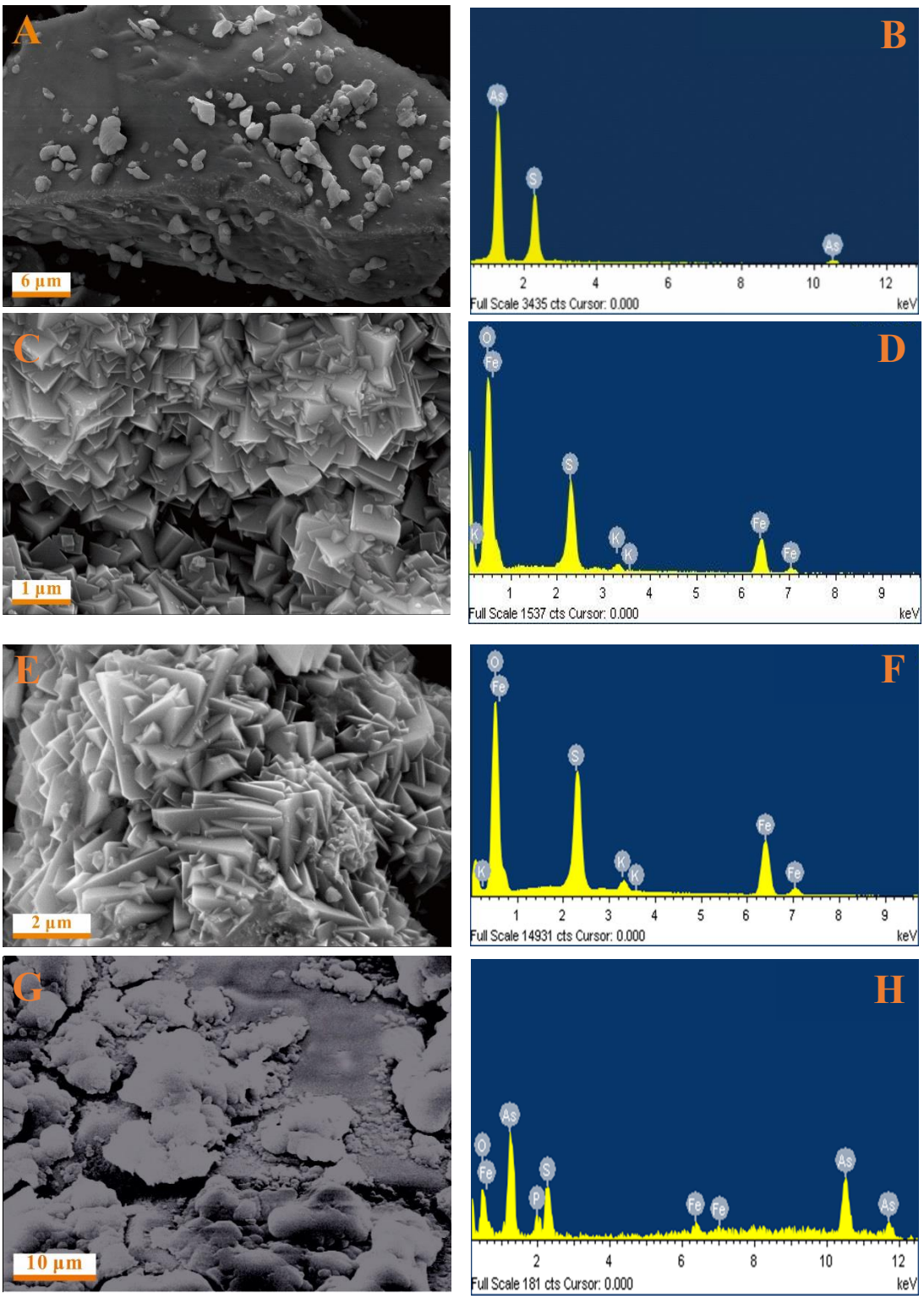

Fig. 5 SEM-EDX images of incubation products in control (A, B), 0 g (C, D), 0.2 g (E, F) and 2.0 g ZVI (G, H) systems after stage III.

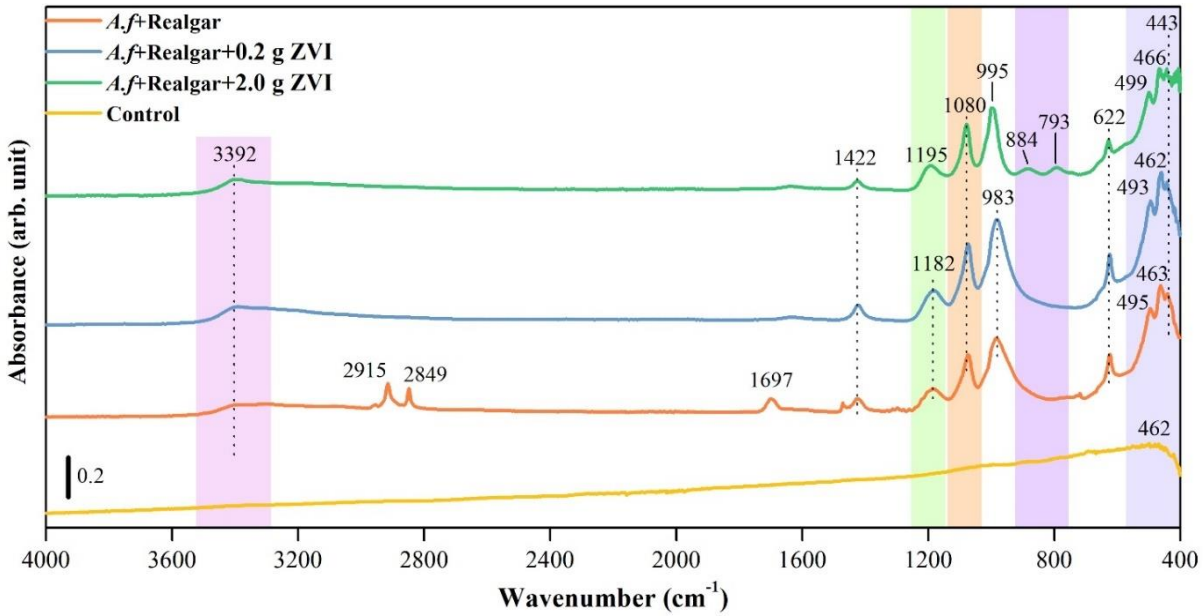

Fig. 6 ATR-FTIR spectra of solid products of the realgar dissolution experiments with and without ZVI after stage III.

The nature of the secondary surface precipitates was further characterized using ATR-FTIR (Fig. 6). The data suggested that the precipitates were composed mainly of four groups of surface-bound species: sulfate compounds, Fe oxyhydroxides, organic matter derived from bacteria residues and water molecules bound to oxidization products. The peak at 3392 cm^{-1} corresponded to bulk H_2O/OH stretching vibrations, as observed for scorodite at ~3300 cm^{-1} and for ferrihydrite at ~3380 cm^{-1} (Cornell, 2004; Wang et al., 2009). The strong peaks at 1195 cm^{-1} and 995 cm^{-1} were assigned to SO_4 asymmetric stretching vibrations (υ_3) and symmetric stretching vibration (υ_1), respectively, whereas the SO_4 in-plane asymmetric bending vibration (υ_4) and weak symmetric bending vibration (υ_2) appeared at 622 cm^{-1} and 443 cm^{-1} with ZVI addition (Moraes and Nart, 1999; Lane et al., 2015). Small peaks at 793 cm^{-1} and 884 cm^{-1} were observed only in 2.0 g ZVI experiment, which were assigned to As-O-Fe complexes (Jia et al., 2007; Guan et al., 2008; Adamescu et al., 2010). The band at 1080 cm^{-1} was assigned to jarosite (Bigham and Nordstrom, 2000). The peaks at 460-490 cm^{-1} were assigned to Fe-O adsorption bending vibrations (Ardelean et al., 2008; Tabelin et al., 2016). The

intensity of the As-O-Fe complexes and Fe-O absorption bands increased with the amount of ZVI, suggesting that the abundance of mixed As(III)/As(V)-Fe oxyhydroxide (and possibly Fe oxyhydroxy sulfate) compounds was related to the amount of ZVI used. The band at 1422 cm^{-1} was assigned to the C=O and C-H deformation modes of organic matter, which might derive from bacteria residues, representing metabolic products formed by the cells (Litescu et al., 2012).

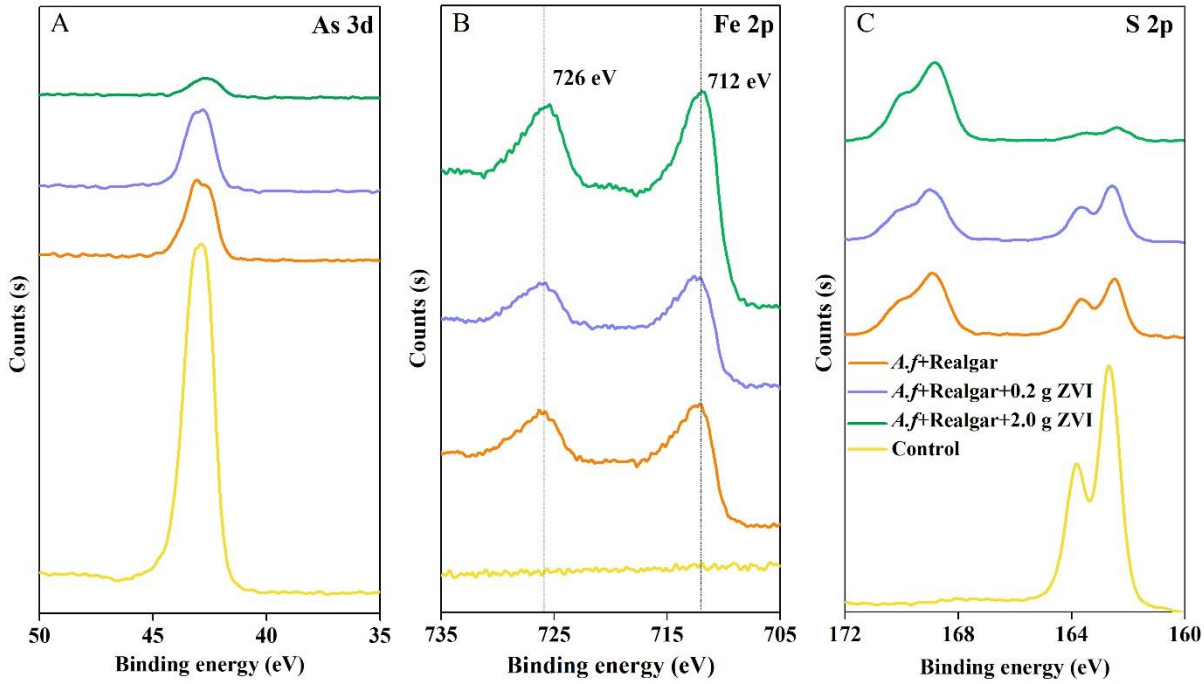

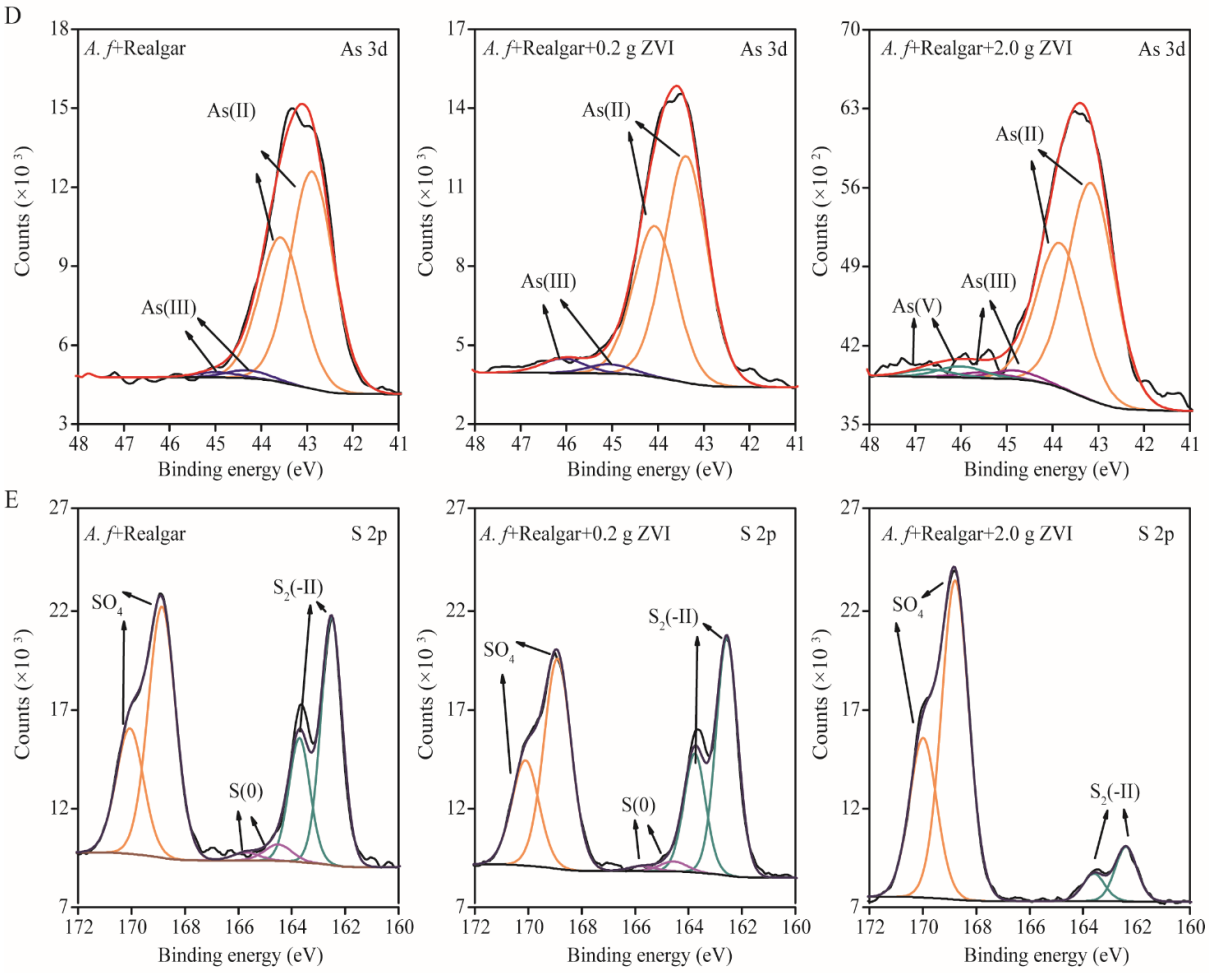

Fig. 7 XPS spectra in As 3d (A, D), Fe 2p (B) and S 2p (C, E) regions of solid products after realgar dissolution in the 0 g, 0.2 g and 2.0 g ZVI experiments after stage III. The As 3d spin orbit-split doublets were fixed of 3:2 at 0.70 eV, and the S 2p spin orbit-split doublets were fixed of 2:1 at 1.2 eV.

The surface of the solids was characterized by XPS to determine the oxidation states of Fe, As and S (Fig. 7 A-C, Table S2). The As 3d spectra were fitted by As $3d_{5/2}$ and As $3d_{3/2}$ doublets with an intensity ratio of 3:2 and spin-orbit splitting of 0.7 eV. The S 2p spectra were fitted by S $2p_{3/2}$ and S $2p_{1/2}$ doublets with an intensity ratio of 2:1 at 1.2 eV. The valence of As in the control experiment was As(II), as suggested by the strong intense As 3d peak that is related to the density of As(II) (Fig. 7A). The decrease in the As 3d peaks in the experimental systems (Fig. 7A), and small shift to higher binding energies (Fig. 7D), indicated decreases in electron densities around the As atom and partial oxidation of As(II) to As(III), or even to As(V), during the dissolution process. As shown in Fig. 7B,

the Fe peak in the control experiment was invisible, but after ZVI addition, peaks at 712 and 726 eV corresponding to the binding energies of $2p_{3/2}$ and $2p_{1/2}$ of Fe(III) were observed on the solid surface. S 2p spectra can be deconvoluted in to three constituents corresponding bonds such as S_2(-II), S(0) and SO_4, respectively. ZVI addition decreased the peaks of S_2(-II), S(0) while the SO_4 peaks increased (Fig. 7E). All of these XPS analyses further elucidated the formation of mixed As(III)/As(V)-Fe oxyhydroxyide and oxyhydroxy sulfate coatings on the realgar surface.

To further identify whether the amount of ZVI added in the experiments affected the production of As-bearing secondary precipitates, the reaction products of each stage were measured for As fractionation via selective extraction. As shown in Fig. S4 and Table S3, arsenic concentrations in crystallized iron oxyhydroxides (F3) were significantly higher than in the other two fractions (F1 and F2) during the entire incubation period. In addition, the amount of As in F3 increased along with the amount of ZVI used (17, 21 and 18 mg kg^{-1} with 0 g ZVI *vs.* 33, 62 and 58 mg kg^{-1} with 2.0 g ZVI at each stage). High ZVI addition in the experiments resulted in higher production of amorphous and crystalline mixed As(III)/As(V)-Fe oxyhydroxides or oxyhydroxy sulfates.

3.4 Mechanisms of realgar dissolution with and without ZVI

3.4.1. 0 g ZVI experiments

During the 0 g ZVI experiments, the Fe(II) in bacterial medium was likely oxidized to Fe(III) by dissolved O_2 or *A. ferrooxidans* (Eq. (1)):

$$Fe^{2+} \rightarrow Fe^{3+} + e^{-} \quad (1)$$

Realgar can be dissolved by H_2O (Eq. (2)). The biogenic Fe(III) produced by *A. ferrooxidans* can also accelerate realgar oxidation (Eq. (3)), and the released elemental S can be further oxidized to SO_4^{2-} (Eq. (4)):

$$As_2S_2 + 14H_2O \rightarrow 2H_3AsO_3 + 2HSO_4^- + 20H^+ + 18e^- \quad (2)$$

$$As_4S_4 + 12Fe^{3+} + 12H_2O \rightarrow 4H_3AsO_3 + 4S + 12Fe^{2+} + 12H^+ \quad (3)$$

$$2S + 3O_2 + H_2O \rightarrow 2SO_4^{2-} + 4H^+ \quad (4)$$

As(II) does not form aqueous species, so in order for arsenous acid to be a product of this reaction, the As(II) in realgar must have been oxidized to As(III). This was confirmed by the XPS results (Fig. 7D). Lengke and Tempel (2003, 2005) have noted that this may occur within the realgar structure itself, and Naumov et al. (2007) suggested the process might be due to photo-induced reaction of As(II) with oxygen. The As(III) released in Eq. (2) was then oxidized to As(V) in the presence of *A. ferrooxidans* (Eq. (5)), as suggested by the increases in As(V) as the experiments proceeded (Fig. 3). This appeared to have a relatively slow process in the 0 g ZVI experiments, since there was a large proportion of As(III) still in solution remaining at 7 d of Stage I (Fig. 3):

$$H_3AsO_3 + H_2O \xrightarrow{A.\ ferroxidans} H_3AsO_4 + 2H^+ + 2e^- \quad (5)$$

The decline in Fe(T) corresponding with As(T) (Fig. 2, Fig. S5) over the 7 d in Stage I suggested that As-Fe complexes such as Fe oxyhydroxides, Fe arsenates or jarosite formed (Eqs. (6)-(8)). This hypothesis can be confirmed by the color change of precipitates (Fig. 4, Fig. S3) and the SEM-EDX (Fig. 5), ATR-FTIR (Fig. 6), XPS (Fig. 7) and selective chemical extraction results (Fig. S4; Table S3):

$$Fe^{3+} + 3H_2O \rightarrow Fe(OH)_3 + 3H^+ \quad (6)$$

$$Fe^{3+} + H_3ASO_4 + 2H_2O \rightarrow FeAsO_4 \cdot 2H_2O + 3H^+ \quad (7)$$

$$3Fe^{3+} + K^+ + 2SO_4^{2-} + 6H_2O \rightarrow KFe_3(SO_4)_2(OH)_6 + 6H^+ \quad (8)$$

The persistence of As(T) in solution in Stage I while Fe(T) declined (Fig. 2) may be due to the abundant As(III) present (Fig. 3) not absorbing or not being incorporating as well as As(V) in the neo-formed Fe oxyhdyroxides and oxyhydroxy sulfate solids. The lesser affinity of Fe(III) phases for As(III) compared to As(V) in the pH range of our experiments has been well-documented in previous

work (And and Hering, 2003). The decreases in As(T) at 7 d of Stage I (Fig. 2), concomitant with increases in As(V) (Fig. 3), suggest that this As was removed from solution by sorption of the arsenate to amorphous iron oxyhydroxides or hydroxy sulfates. These precipitates likely coated on the realgar surface, restricting its further dissolution. Burnol et al. (2007) pointed out that re-sorption of released As(V) is the main reason for incongruent release of As from As-adsorbed and co-precipitated ferrihydrite. The similar patterns of As(T) and Fe(T) in Stage I (Fig. 2) occurred once the abundance of the secondary Fe precipitates reached a critical threshold.

Stage II As(T) and Fe(T) concentrations were relatively low compared to those in Stage I (Fig. 2). This suggested either that realgar oxidation occurred to a lesser degree in Stage II, or that this process did occur, and the As released from realgar oxidation was immediately absorbed to, or co-precipitated with, secondary iron precipitates. As in Stage I, the dominant species of As released at 1 d of Stage II was As(III) (Fig. 3), it was unlikely that a significant proportion of this As(III) was absorbed to the Fe precipitates. Therefore, realgar oxidation was likely inhibited in Stage II. The increases in As(T) and Fe(T) at the end of Stage II (Fig. 2, Fig. S5) could have been due to the partial dissolution of amorphous Fe-As oxyhydroxides or hydroxy sulfates formed earlier in the experiment in response to declining pH (Alabed et al., 2007), or to a lack of nucleation sites for fresh Fe-As hydroxy sulfates coated on realgar surface. Increases in Fe(T) at the beginning of Stage III may have been due to the inputs of fresh microbial medium between the stages.

The declines in pH seen over the 7 d of Stages I to III were likely due to the generation of protons during realgar oxidation (Eq. (2)-(3)), As(III) oxidation (Eq. (5)) and secondary Fe mineral formation (Eq. (6)-(8)).

3.4.2. 0.2 g and 2.0 ZVI experiments

The mechanisms described above for realgar oxidation in the presence of *A. ferrooxidans* likely also occurred in the 0.2 g and 2.0 g ZVI experiments, but the addition of the ZVI introduced further complexity to the system. The significant pH and Eh changes in Stages I and II of the 2.0 ZVI experiment were primarily due to the consumption of protons and oxygen, respectively, during the abiotic reaction of ZVI with oxygen (Eq. (9)) (Su and Puls, 2001; Mkandawire and Dudel, 2005; Xie et al., 2016):

$$2Fe + 2O_2 + 4H^+ \rightarrow 2Fe^{2+} + 2H_2O \quad (9)$$

The lack of significant pH and Eh changes in the 0.2 g ZVI experiments might be due to the low quantities of ZVI present and the ability of the system to buffer minor changes. The Fe(II) generated in Eq. (8) would have been an additional source of Fe(II) for *A. ferrooxidans* to generate Fe(III) (Eq. (1)), which could in turn form additional Fe(III) precipitates (Eq. (6)-(8)) evidenced by ATR-FTIR, XPS and selective extraction data. Lengke and Tempel (2003) showed that the degree of realgar oxidation and extent of As release will increase with decreasing pH. Thus, decreases in pH observed towards the end of all the experimental stages (Fig. 1) likely enhanced As release, but the released As was then attenuated via sorption or co-precipitation of the As to secondary Fe precipitates (Eq. (6)-(8)).

The increase in As(III) in day 7 of the 2.0 g ZVI experiments (Fig. 3) indicated that some of the As(V) produced by oxidation of As(III) was reduced back to As(III). This likely occurred by the reduction of the As(V) by the ZVI (Burlo et al., 1999; Chunming Su and Puls, 2001; Su and Puls, 2001), which in turn oxidized, producing additional Fe(II). This process, shown in Eq. (10), would have led to further generation of Fe(II), which would in turn have oxidized to Fe(III) to generate more secondary As-Fe phases (Eq. (6)-(8)). This is confirmed by the selective extraction results.

$$2Fe + H_3ASO_4 + 2H^+ \rightarrow 2Fe^{2+} + H_3ASO_3 + H_2O \quad (10)$$

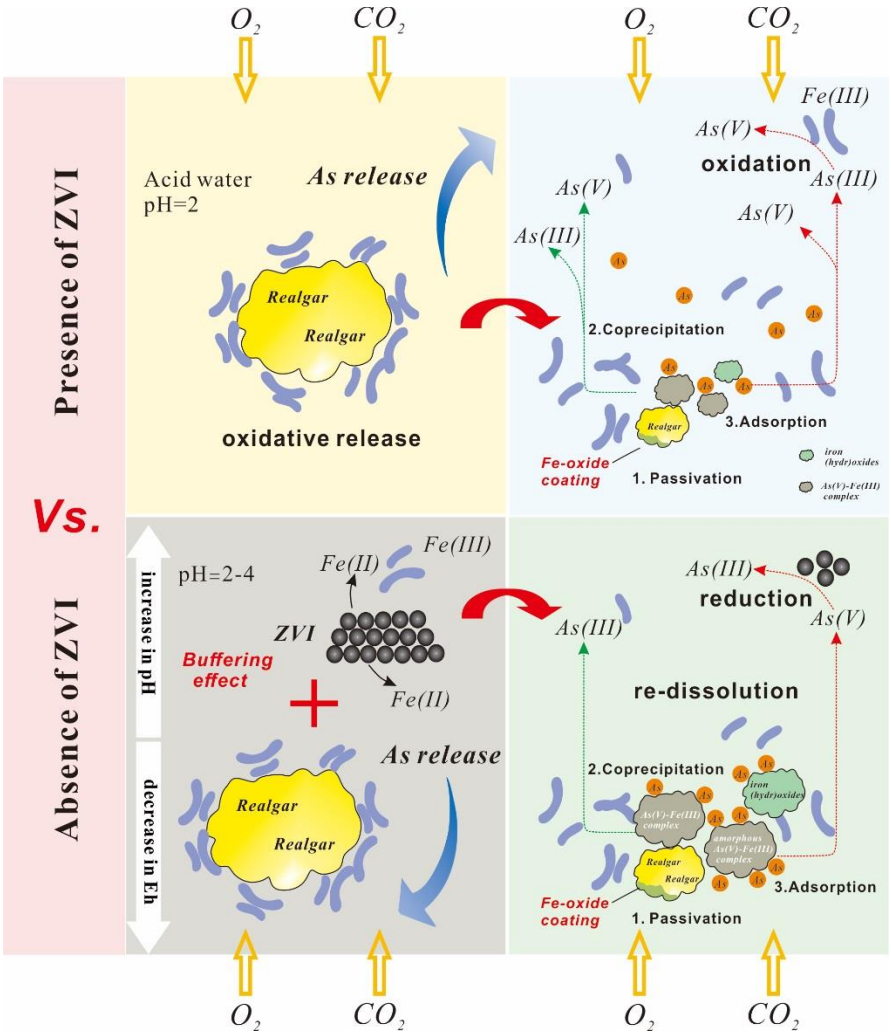

Fig. 8 Schematic of realgar dissolution by *A. ferrooxidans* in the absence and presence of ZVI.

Our schematic model for realgar dissolution by *A. ferrooxidans* in the presence and absence of ZVI, discussed above, is shown in Fig. 8.

3.5 Environmental Implications

The village of Shimen in Hunan Province, China, is grossly contaminated with As and has been described as a 'Cancer Village' (Dong et al., 2014; Chen et al., 2017). The mine was closed by the Chinese government in 2011 due to serious As poisoning in the surrounding area (Fan et al., 2018).

Arsenic concentrations of Shimen tailings pore waters vary from 0.5 to 782 mg L^{-1} (Fan et al., 2018). These waters are the main As contamination source to the Shishui River. The As-containing tailings in this area have low Fe concentrations (1.41-4.23 wt.% Fe_2O_3) compared to those of arsenopyrite-rich tailings, such as in the Yao Gang Xian mine, China (28.57 wt.% Fe_2O_3) (Liu et al., 2015). Realgar ores have also been mined in many other parts of China (e.g., Nanhua, Dali, Sinan, Ningshan) and the rest of the world (e.g., USA, Russia, Turkey, France) (Migon and Mori, 1999; Tempel et al., 2000; Çolak et al., 2003; Wu et al., 2017). Huge quantities of realgar-rich tailings and related wastes are deposited in open-air impoundments in these areas, and many have only been treated by addition of a soil cover. Based on our results, we suggest that a combination of commercial or slag ZVI dust and *A. ferrooxidans* might be used to treat these *in-situ* realgar tailings to reduce As release in these areas. Increases in As(T) release at the end of Stages II and III of the experiments (Fig. 2), however, indicate that the effectiveness of such a treatment scheme would need to be monitored in the long-term.

4. Conclusions

This study examined gradient levels (0 g, 0.2 g, 2 g) of exogenous zerovalent iron (ZVI) addition on the realgar dissolution by *A. ferrooxidans*. Our major findings are depicted schematically in Fig. 8 and are summarized as follows:

1) Realgar dissolution by *A. ferrooxidans* results in decreases in solution pH and increases in Eh. However, high amounts of ZVI (2.0 g) addition initially causes increases in pH and decreases in Eh due to ZVI dissolution at first, but as realgar oxidation proceeds, these trends are reversed.
2) The As(II) in realgar is oxidized to As(III), and this it released to solution as dissolution proceeds. Most released As(III) is then oxidized to As(V), although with some of the As(V) is reduced back to As(III) by ZVI in the high (2.0 g) experiment.

3) High amounts of ZVI addition (2.0 g in this study) significantly decreases As release (down to 0.2 mg L^{-1} in this study) compared to experiments using *A. ferrooxidans* only (0 g ZVI; to 30 mg L^{-1}), although As release in the latter also decreases over time. Arsenic attenuation is attributed to uptake of mainly As(V) by secondary Fe oxyhydroxides and hydroxy sulfates, or by passivation of the realgar surface. Higher amounts of crystalline As-bearing Fe oxyhydroxides (F3) are produced in high ZVI (2.0 g) experiments (33, 62 and 58 mg kg^{-1} per stage) compared with the 0 g ZVI addition experiments (17, 21 and 18 mg kg^{-1} per stage).

4) A combination of commercial or slag ZVI dust and *A. ferroxidans* could be used to treat these *in-situ* realgar tailings to reduce As release, although its long-term effects need to be monitored.

6. Acknowledgements

This study was supported by the National Natural Science Foundation of China (Grant No. 4177236) and National Key R&D Program of China (2016YFC0502204).

References

Adamescu, A., Mitchell, W., Hamilton, I.P., Alabadleh, H.A., 2010. Insights into the surface complexation of dimethylarsinic acid on iron (oxyhydr)oxides from ATR-FTIR studies and quantum chemical calculations. Environ. Sci. Technol. 44, 7802-7807.

Alabed, S.R., Jegadeesan, G., Purandare, J., Allen, D., 2007. Arsenic release from iron rich mineral processing waste: Influence of pH and redox potential. Chemosphere 66, 775-782.

And, S.D., Hering, J.G., 2003. Comparison of arsenic(V) and arsenic(III) sorption onto iron oxide minerals: Implications for arsenic mobility. Environ. Sci. Technol. 37, 4182-4189.

Ardelean, I., Toderas, M., Paşcuţa, P., 2008. Structural study of the Fe_2O_3–B_2O_3–BaO glass system by FTIR spectroscopy. Mod. Phys. Lett. B 17, 1175-1179.

Barrett, J., Ewart, D.K., Hughes, M.N., Poole, R.K., 1993. Chemical and biological pathways in the bacterial oxidation of arsenopyrite. FEMS Microbiol. Rev. 11, 57-62.

Bigham, J.M., Nordstrom, D.K., 2000. Iron and aluminum hydroxysulfates from acid sulfate waters. Rev. Mineral. Geochem. 40, 351-403.

Burlo, F., Carbonell-Barrchina, A., Jugsujinda, A., Anurakpongsatorn, P., Delaune, R.D., Sirisukhodom, S., 1999. The influence of redox chemistry and pH on chemically active forms of arsenic in sewage sludge-amended soil. Environ. Int.

25, 613-618.
Burnol, A., Garrido, F., Baranger, P., Joulian, C., Dictor, M.C., Bodénan, F., Morin, G., Charlet, L., 2007. Decoupling of arsenic and iron release from ferrihydrite suspension under reducing conditions: a biogeochemical model. Geochem. Trans. 8, 12.
Burton, E.D., Johnston, S.G., Kraal, P., Bush, R.T., Claff, S., 2013. Sulfate availability drives divergent evolution of arsenic speciation during microbially mediated reductive transformation of schwertmannite. Environ. Sci. Technol. 47, 2221-2229.
Chen, P., Yan, L., Leng, F., Nan, W., Yue, X., Zheng, Y., Feng, N., Li, H., 2011. Bioleaching of realgar by Acidithiobacillus ferrooxidans using ferrous iron and elemental sulfur as the sole and mixed energy sources. Bioresour. Technol. 102, 3260-3267.
Chen, Y.T., Li, J.T., Chen, L.X., Hua, Z.S., Huang, L.N., Liu, J., Xu, B.B., Liao, B., Shu, W.S., 2014. Biogeochemical processes governing natural pyrite oxidation and release of acid metalliferous drainage. Environ. Sci. Technol. 48, 5537-5545.
Chen, Z., Wang, Y., Jiang, X., Fu, D., Xia, D., Wang, H., Dong, G., Li, Q., 2017. Dual roles of AQDS as electron shuttles for microbes and dissolved organic matter involved in arsenic and iron mobilization in the arsenic-rich sediment. Sci. Total Environ. 574, 1684-1694.
Chunming Su, A., Puls, R.W., 2001. Arsenate and arsenite removal by zerovalent iron: Kinetics, redox transformation, and implications for in situ groundwater remediation. Environ. Sci. Technol. 35, 1487-1492.
Çolak, M., Gemici, Ü., Tarcan, G., 2003. The effects of colemanite deposits on the arsenic concentrations of soil and ground water in Igdeköy-Emet, Kütahya, Turkey. Water Air Soil Pollut. 149, 127-143.
Corkhill, C.L., Vaughan, D.J., 2009. Arsenopyrite oxidation – A review. Appl. Geochem. 24, 2342-2361.
Cornell, R.M., 2004. The Iron Oxides: Structure, Properties, Reactions, Occurences and Uses, Second Edition.
Cullen, W.R., Reimer, K.J., 1989. ChemInform Abstract: Arsenic speciation in the environment. Cheminform 20.
Dixit, S., Hering, J.G., 2003. Comparison of arsenic(V) and arsenic(III) sorption onto iron oxide minerals: Implications for arsenic mobility. Environ. Sci. Technol. 37, 4182-4189.
Dong, G., Huang, Y., Yu, Q., Wang, Y., Wang, H., He, N., Li, Q., 2014. Role of nanoparticles in controlling arsenic mobilization from sediments near a realgar tailing. Environ. Sci. Technol. 48, 7469-7476.
Egal, M., Casiot, C., Morin, G., Parmentier, M., Bruneel, O., Lebrun, S., Elbaz-Poulichet, F., 2009. Kinetic control on the formation of tooeleite, schwertmannite and jarosite by Acidithiobacillus ferrooxidans strains in an As(III)-rich acid mine water. Chem. Geol. 265, 432-441.
Fan, L., Zhao, F., Liu, J., Frost, R.L., 2018. The As behavior of natural arsenical-containing colloidal ferric oxyhydroxide reacted with sulfate reducing bacteria. Chem. Eng. J. 332, 183-191.
Gonzalezcontreras, P., Weijma, J., Buisman, C.J.N., 2012. Bioscorodite crystallization in an airlift reactor for arsenic removal. Crystal Growth Des. 12, 2669-2706.
Gonzalezcontreras, P., Weijma, J., Weijden, R.V.D., Buisman, C.J.N., 2010. Biogenic scorodite crystallization by Acidianus sulfidivorans for arsenic removal. Environ. Sci. Technol. 44, 675-680.
Guan, X.H., Wang, J., Chusuei, C.C., 2008. Removal of arsenic from water using granular ferric hydroxide: macroscopic and microscopic studies. J. Hazard. Mater. 156, 178-185.
Jia, Y., Xu, L., Wang, X., Demopoulos, G.P., 2007. Infrared spectroscopic and X-ray diffraction characterization of the nature of adsorbed arsenate on ferrihydrite. Geochim. Cosmochim. Acta 71, 1643-1654.
Johnston, S.G., Burton, E.D., Keene, A.F., Planer-Friedrich, B., Voegelin, A., Blackford, M.G., Lumpkin, G.R., 2012. Arsenic mobilization and iron transformations during sulfidization of As(V)-bearing jarosite. Chem. Geol. 334, 9-24.
Johnston, S.G., Keene, A.F., Burton, E.D., Bush, R.T., Sullivan, L.A., 2011. Iron and arsenic cycling in intertidal surface sediments during wetland remediation. Environ. Sci. Technol. 45, 2179-2185.
Jones, R.A., Koval, S.F., Nesbitt, H.W., 2003. Surface alteration of arsenopyrite (FeAsS) by Thiobacillus ferrooxidans. Geochim. Cosmochim. Acta 67, 955-965.

Ko, M.S., Park, H.S., Kim, K.W., Lee, J.U., 2013. The role of Acidithiobacillus ferrooxidans and Acidithiobacillus thiooxidans in arsenic bioleaching from soil. Environ. Geochem. Health 35, 727-733.

Kuijae, L., Yunho, L., Jeyong, Y., Kamalakannan, S., Seungmoon, P., Byungtaek, O., 2009. Assessment of zero-valent iron as a permeable reactive barrier for long-term removal of arsenic compounds from synthetic water. Environ. Technol. 30, 1425-1434.

Kyono, A., Kimata, M., Hatta, T., 2005. Light-induced degradation dynamics in realgar: in situ structural investigation using single-crystal X-ray diffraction study and X-ray photoelectron spectroscopy. Am. Mineral. 90, 1563-1570.

Lane, M.D., Bishop, J.L., Dyar, M.D., Hiroi, T., Mertzman, S.A., Bish, D.L., King, P.L., Rogers, A.D., 2015. Mid-infrared emission spectroscopy and visible/near-infrared reflectance spectroscopy of Fe-sulfate minerals. Am. Mineral. 100, 66-82.

Lengke, M.F., Tempel, R.N., 2003. Natural realgar and amorphous AsS oxidation kinetics. Geochim. Cosmochim. Acta 67, 859-871.

Lengke, M.F., Tempel, R.N., 2005. Geochemical modeling of arsenic sulfide oxidation kinetics in a mining environment. Geochim. Cosmochim. Acta 69, 341-356.

Liang, Y., Min, X., Chai, L., Wang, M., Liyang, W., Pan, Q., Okido, M., 2017. Stabilization of arsenic sludge with mechanochemically modified zero valent iron. Chemosphere 168, 1142-1151.

Litescu, S.C., Teodor, E.D., Truica, G.I., Tache, A., Radu, G.L., 2012. Fourier Transform Infrared Spectroscopy - Useful Analytical Tool for Non-Destructive Analysis. InTech, http://cdn.intechopen.com/pdfs/36183/InTech-Fourier_transform_infrared_spectroscopy_useful_analytical_tool_for_non_destructive_analysis.pdf Accessed 20 May 2018.

Liu, Z., Lei, H.-Y., Bai, T., Wang, W.-Z., Chen, K., Chen, J.-J., Hu, Q.-W., 2015. Microwave-assisted arsenic removal and the magnetic effects of typical arsenopyrite-bearing mine tailings. Chem. Eng. J. 272, 1-11.

Lu, X., Wang, H., 2012. Microbial oxidation of sulfide tailings and the environmental consequences. Elements 8, 119-124.

Macur, R.E., Wheeler, J.T., Mcdermott, T.R., Inskeep, W.P., 2001. Microbial populations associated with the reduction and enhanced mobilization of arsenic in mine tailings. Environ. Sci. Technol. 35, 3676-3682.

Meruane, G., Vargas, T., 2003. Bacterial oxidation of ferrous iron by Acidithiobacillus ferrooxidans in the pH range 2.5–7.0. Hydrometallurgy 71, 149-158.

Migon, C., Mori, C., 1999. Arsenic and antimony release from sediments in a Mediterranean estuary. Hydrobiologia 392, 81-88.

Mkandawire, M., Dudel, E.G., 2005. Accumulation of arsenic in Lemna gibba L. (duckweed) in tailing waters of two abandoned uranium mining sites in Saxony, Germany. Sci. Total Environ. 336, 81-89.

Moraes, I.R.D., Nart, F.C., 1999. Sulfate ions adsorbed on Au(hkl) electrodes: in situ vibrational spectroscopy 1. J. Electroanal. Chem. 461, 110-120.

Naumov, P., Makreski, P., Jovanovski, G., 2007. Direct atomic scale observation of linkage isomerization of As_4S_4 clusters during the photoinduced transition of realgar to pararealgar. Inorg. Chem. 46, 10624-10631.

Neil, C.W., Jun, Y.S., 2016. Fe^{3+} addition promotes arsenopyrite dissolution and iron(III) (hydr)oxide formation and phase transformation. Environ. Sci. Technol. Lett. 3, 30-35.

Nesbitt, H.W., Muir, I.J., 1998. Oxidation states and speciation of secondary products on pyrite and arsenopyrite reacted with mine waste waters and air. Mineral. Petrol. 62, 123-144.

Nordstrom, D.K., Alpers, C.N., 1999. Negative pH, efflorescent mineralogy, and consequences for environmental restoration at the Iron Mountain Superfund site, California. Proc. Natl. Acad. Sci. USA 96, 3455-3462.

Okibe, N., Morishita, S., Tanaka, M., Sasaki, K., Hirajima, T., Hatano, K., Ohata, A., 2017. Bioscorodite crystallization using Acidianus brierleyi : Effects caused by Cu(II) present in As(III)-bearing copper refinery wastewaters. Hydrometallurgy 168, 121-126.

Ouyang, B., Lu, X., Liu, H., Li, J., Zhu, T., Zhu, X., Lu, J., Wang, R., 2014. Reduction of jarosite by Shewanella oneidensis

MR-1 and secondary mineralization. Geochim. Cosmochim. Acta 124, 54-71.
Percak-Dennett, E., He, S., Converse, B., Konishi, H., Xu, H., Corcoran, A., Noguera, D., Chan, C., Bhayyacharyya, A., Borch, T., 2017. Microbial acceleration of aerobic pyrite oxidation at circumneutral pH. Geobiology 15, 690-703.
Qiu, G., Gao, T., Hong, J., Tan, W., Liu, F., Zheng, L., 2017. Mechanisms of arsenic-containing pyrite oxidation by aqueous arsenate under anoxic conditions. Geochim. Cosmochim. Acta 217, 306-319.
Reich, M., Kesler, S.E., Utsunomiya, S., Palenik, C.S., Chryssoulis, S.L., Ewing, R.C., 2005. Solubility of gold in arsenian pyrite. Geochim. Cosmochim. Acta 69, 2781-2796.
Root, R.A., Dixit, S., Campbell, K.M., Jew, A.D., Hering, J.G., O'Day, P.A., 2009. Arsenic sequestration by sorption processes in high-iron sediments. Geochim. Cosmochim. Acta 71, 5782-5803.
Shi, Y., Chen, W.Q., Wu, S., Zhu, Y., 2017. Anthropogenic cycles of arsenic in mainland China: 1990-2010. Environ. Sci. Technol. 51, 1670-1678.
Silverman, M.P., Lundgren, D.G., 1959. Studies on the chemoautotrophic iron bacterium Ferrobacillus ferrooxidans I. An improved medium and a harvesting procedure for securing high cell yields. J. Bacteriol. 77, 642-647.
Singer, P.C., Stumm, W., 1970. Acidic mine drainage: the rate-determining step. Science 167, 1121-1123.
Smedley, P.L., Kinniburgh, D.G., 2002. A review of the source, behaviour and distribution of arsenic in natural waters. Appl. Geochem. 17, 517-568.
Smith, A.H., Hopenhaynrich, C., Bates, M.N., Goeden, H.M., Hertzpicciotto, I., Duggan, H.M., Wood, R., Kosnett, M.J., Smith, M.T., 1992. Cancer risks from arsenic in drinking water. Environ. Health Perspect. 97, 259-267.
Su, C., Puls, R.W., 2001. Arsenate and arsenite removal by zerovalent iron: effects of phosphate, silicate, carbonate, borate, sulfate, chromate, molybdate, and nitrate, relative to chloride. Environ. Sci. Technol. 35, 4562-4568.
Tabelin, C.B., Veerawattananun, S., Ito, M., Hiroyoshi, N., Igarashi, T., 2016. Pyrite oxidation in the presence of hematite and alumina: I. Batch leaching experiments and kinetic modeling calculations. Sci. Total Environ. 580, 687-698.
Tempel, R.N., Shevenell, L.A., Lechler, P., Price, J., 2000. Geochemical modeling approach to predicting arsenic concentrations in a mine pit lake. Appl. Geochem. 15, 475-492.
Tuček, J., Prucek, R., Kolařík, J., Zoppellaro, G., Petr, M., Filip, J., Sharma, V.K., Zbořil, R., 2017. Zero-valent iron nanoparticles reduce arsenites and arsenates to As(0) firmly embedded in core–shell superstructure: Challenging strategy of arsenic treatment under anoxic conditions. ACS Sustain. Chem. Eng. 5, 3027-3038.
Wang, P.X., Wu, X.L., Xue, D.H., Xu, K., Tan, Y., Du, X.B., Li, W.B., 2009. Preparation and characterization of cationic corn starch with a high degree of substitution in dioxane-THF-water media. Carbohydr. Res. 344, 851-855.
Wenzel, W.W., Kirchbaumer, N., Prohaska, T., Stingeder, G., Lombi, E., Adriano, D.C., 2001. Arsenic fractionation in soils using an improved sequential extraction procedure. Anal. Chim. Acta 436, 309-323.
Wu, Y., Zhou, X.Y., Lei, M., Yang, J., Ma, J., Qiao, P.W., Chen, T.B., 2017. Migration and transformation of arsenic: Contamination control and remediation in realgar mining areas. Appl. Geochem. 77, 44-51.
Xie, Y., Dong, H., Zeng, G., Lin, T., Zhao, J., Cong, Z., Deng, J., Zhang, L., Yi, Z., 2016. The interactions between nanoscale zero-valent iron and microbes in the subsurface environment: A review. J. Hazard. Mater. 321, 390-407.
Xie, Y., Dong, H., Zeng, G., Tang, L., Jiang, Z., Zhang, C., Deng, J., Zhang, L., Zhang, Y., 2017. The interactions between nanoscale zero-valent iron and microbes in the subsurface environment: A review. J. Hazard. Mater. 321, 390-407.
Yamaguchi, N., Nakamura, T., Dong, D., Takahashi, Y., Amachi, S., Makino, T., 2011. Arsenic release from flooded paddy soils is influenced by speciation, Eh, pH, and iron dissolution. Chemosphere 83, 925-932.
Yan, L., Hu, H., Zhang, S., Chen, P., Wang, W., Li, H., 2017. Arsenic tolerance and bioleaching from realgar based on response surface methodology by Acidithiobacillus ferrooxidans isolated from Wudalianchi volcanic lake, northeast China. Electron. J. Biotechnol. 25, 50-57.
Zhang, J., Zhang, X., Ni, Y., Yang, X., Li, H., 2007. Bioleaching of arsenic from medicinal realgar by pure and mixed cultures. Process Biochem. 42, 1265-1271.

Supplementary materials

Dissolution of realgar by *Acidithiobacillus ferrooxidans* in the presence and absence of zerovalent iron: Implications for remediation of iron-deficient arsenic-rich tailings

Lijun Fan[1], Fenghua Zhao[1], Jing Liu[2, 3, *], Karen A. Hudson-Edwards[3, *]

[1] College of Geoscience and Surveying Engineering, China University of Mining & Technology, Beijing 100083, China.

[2] The Key Laboratory of Solid Waste Treatment and Resource, Ministry of Education, Southwest University of Science and Technology, 621010 Mianyang China.

[3] Environment & Sustainability Institute and Camborne School of Mines, University of Exeter, Penryn, Cornwall TR10 9DF, UK.

1.1 Selective extraction method

Table S1. Selective extraction procedure and reagents

Step	Extractant	Target phase	Condition	Target species
1	0.05 M KH_2PO_4	Surface-adsorbed As	pH 5.0, 16 h shaking at 20 °C	F1
2	0.2 M NH_4-oxalate buffer	Amorphous Fe (oxyhydr)oxides As	pH 3.25, 4 h shaking at 20 °C in the dark	F2
3	0.2 M NH_4-oxalate buffer + 0.1 M ascorbic acid	Crystallized Fe (oxyhydr)oxides As	pH 3.25, 30 min in a water basin at 96 °C in the light	F3

1) F1: A 10 mL aliquot of 1 M KH_2PO_4 at pH 5.0 was added to 50 mL polyethylene centrifuge tubes containing 0.25 g solid. Samples were prepared in duplicate. The tubes were continuously shaken for16 h and centrifuged for 10 min at 10,000 rpm, after which the separated extraction solution was carefully pipetted off. The residue was rinsed with 19 mL deionized water, centrifuged, and decanted.

2) F2: The residue from Step 1 was extracted with 10 mL 0.2 M NH_4-oxalate buffer in 50 mL polyethylene centrifuge tubes. Samples were shaken for 4 h and then treated in the same manner described in Step 1.

3) F3: The residue from Step 2 was extracted with 10 mL NH_4-oxalate buffer + 0.1 M ascorbic acid in a water bath at 96°C for 30 min. The extraction was piped off in the same manner described in Step 1.

1.2 XRD analysis

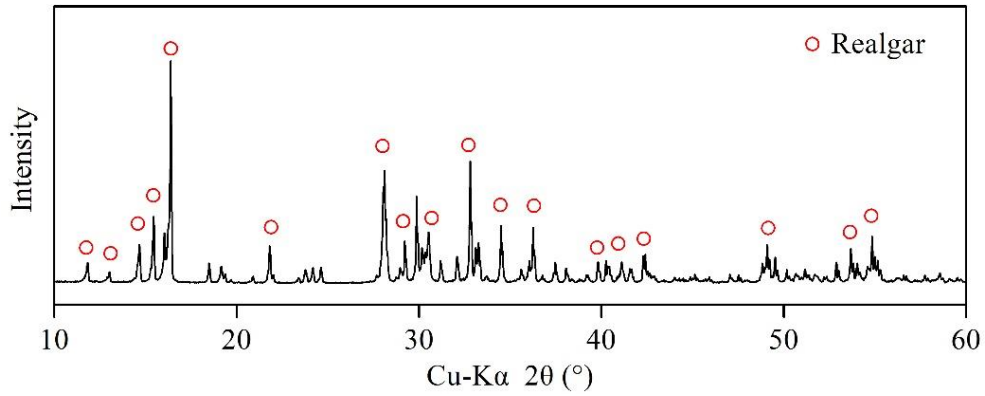

Fig. S1 XRD pattern of the raw realgar.

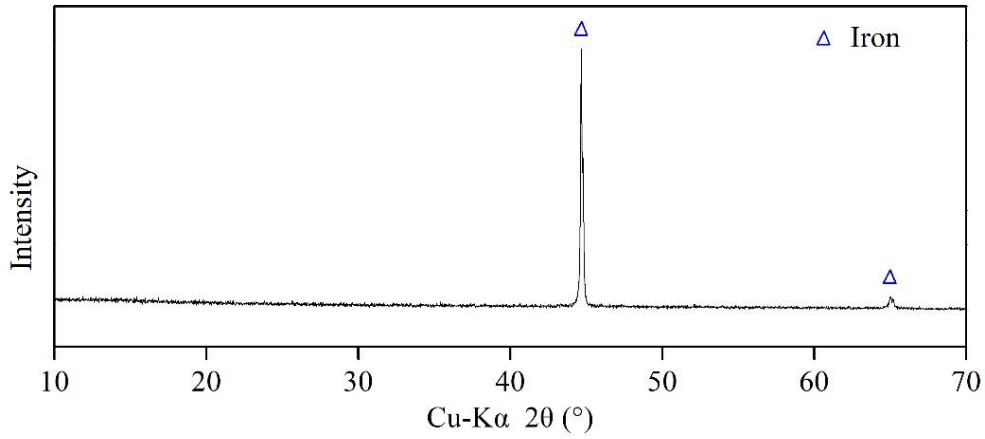

Fig. S2 XRD pattern of the ZVI power.

1.3 The color change of the experiment

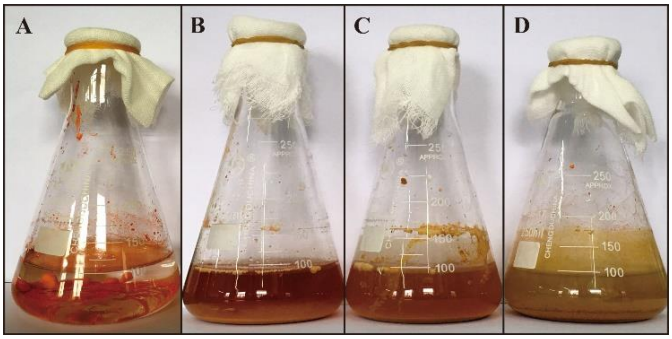

Fig. S3 Visible changes in color during oxidative dissolution of realgar by *A. ferrooxidans* in three ZVI treatments. (A: control, B: 0 g ZVI, C: 0.2 g ZVI; 2.0 g ZVI).

1.4 XPS analysis

Table S2 Iron, arsenic and sulfur peak XPS parameters and chemical states of solid products after realgar dissolution in different ZVI amendments.

Spectral peak	Binding energy (eV)	FWHM	Chemical state
	162.4±0.2	1.0	S_2(-II)
S $2p_{3/2}$	164.4±0.2	1.2	S(0)
	168.8±0.2	1.2	SO_4
	163.6±0.2	1.0	S_2(-II)
S $2p_{1/2}$	165.6±0.2	1.2	S(0)
	170.0±0.2	1.2	SO_4
	42.7±0.2	1.1	As(II)
As $3d_{5/2}$	44.4±0.2	1.1	As(III)
	45.3±0.2	1.1	As(V)
	43.5±0.2	1.1	As(II)
As $3d_{3/2}$	45.0±0.2	1.1	As(III)
	46.2±0.2	1.1	As(V)

1.5 Selective extraction results

Table S3 Arsenic concentrations in the selective extraction F1, F2 and F3 steps in the different ZVI amendments.

	ZVI (g)	F1 (mg kg^{-1})	F2 (mg kg^{-1})	F3 (mg kg^{-1})
Stage I	0	6.52	10.58	16.64
	0.2	2.25	24.36	23.16
	2.0	17.15	28.72	33.40
Stage II	0	9.53	3.78	7.82
	0.2	3.15	6.33	5.96
	2.0	21.29	46.57	61.61
Stage III	0	5.70	2.04	4.09
	0.2	1.80	7.28	9.19
	2.0	17.55	33.63	57.95

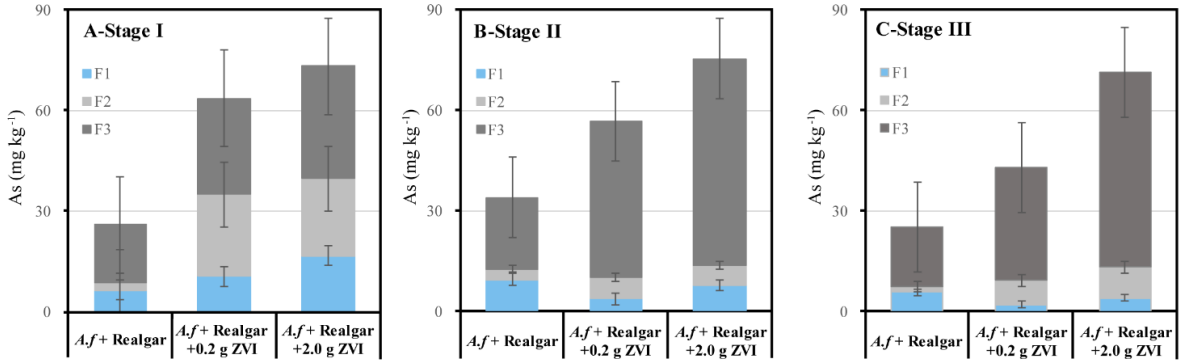

Fig. S4 As distribution identified through selective extraction performed on different incubation systems. Surface-adsorbed (F1), Amorphous iron oxyhydroxides As (F2), crystallized iron oxyhydroxides As (F3) phases were extracted on the 7th day of each stage. Error bars denote standard deviations (n = 3).

1.6 The relationship between As(T) and Fe(T)

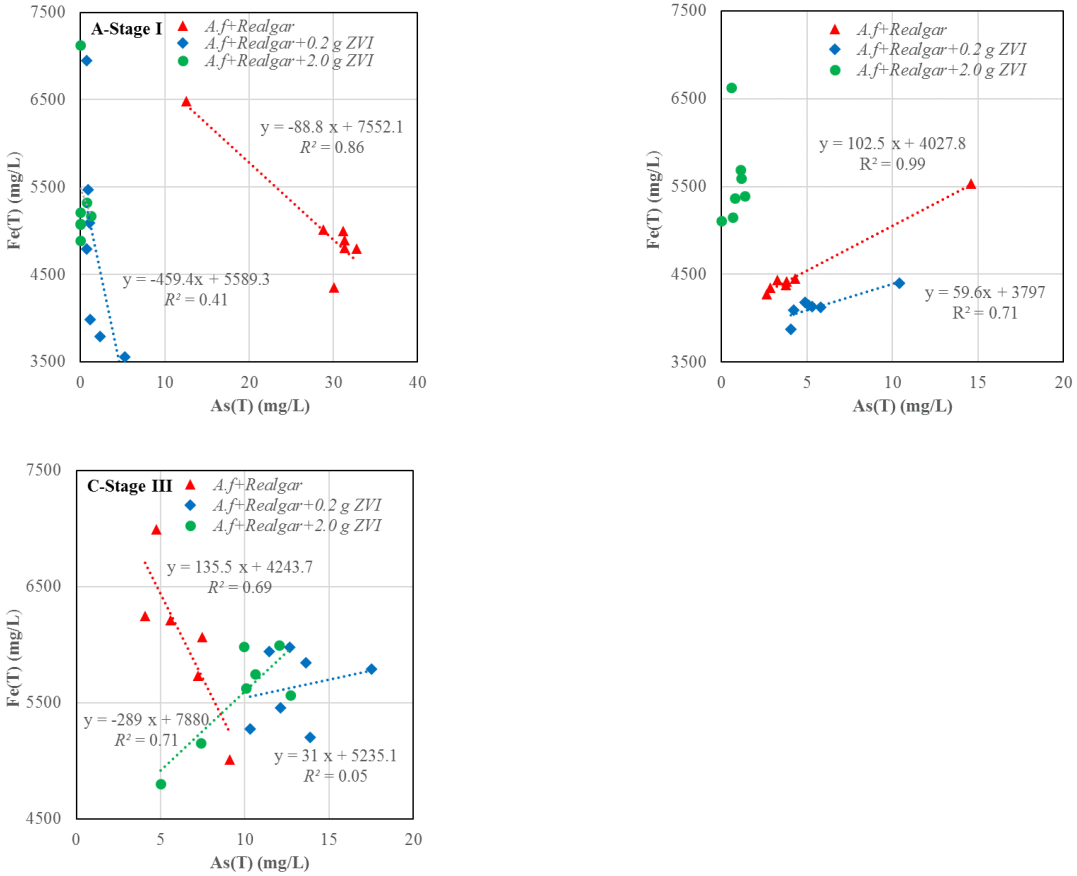

Fig. S5 Relationship between aqueous As(T) and Fe(T) in the 0 g, 0.2 g and 2.0 g ZVI amended experiments in three stages (As(T): total arsenic; Fe(T): total iron).

The data were processed using Microsoft Excel software 2016. A liner regression was employed to compare the correlation between soluble As(T) and Fe(T) (Fig. S5). Strong correlations (R^2 = 0.41-0.99) were observed between aqueous As(T) and Fe(T) in the 0, 0.2 g treatments in stage I and II. In stage III the correlations were complex, suggesting that two As release mechanisms may exist.

1.7 As(III) and As(V) concentrations and proportions of the three stages

Table S4 Arsenic species distribution (mg L^{-1}) during realgar dissolution in different ZVI amendments of the three stages.

Condition	Stage I (mg L^{-1})		Stage II (mg L^{-1})		Stage III (mg L^{-1})	
	As(III)	As(V)	As(III)	As(V)	As(III)	As(V)
Control-1d	12.86	1.39	4.22	0.58	2.10	0.42
Control-7d	32.60	4.26	17.93	1.86	10.36	0.79
***A.f*+Realgar+0 g ZVI-1d**	10.51	2.83	3.14	0.57	3.80	0.86
***A.f*+Realgar+0 g ZVI-7d**	15.24	15.16	0.80	6.74	0.77	5.52
***A.f*+Realgar+0.2 g ZVI-1d**	0.66	0.14	4.14	0.72	9.31	1.16
***A.f*+Realgar+0.2 g ZVI-7d**	0.10	4.99	1.70	5.41	3.89	8.18
***A.f*+Realgar+2.0 g ZVI-1d**	0.07	0.14	0.39	0.13	4.32	0.93
***A.f*+Realgar+2.0 g ZVI-7d**	0.09	0.40	0.34	0.20	6.11	3.65

Table S5 Arsenic species proportion (%) during realgar dissolution in different ZVI amendments of the three stages.

Condition	Stage I (%)		Stage II (%)		Stage III (%)	
	As(III)/As(T)	As(V)/As(T)	As(III)/As(T)	As(V)/As(T)	As(III)/As(T)	As(V)/As(T)
Control-1d	90	10	88	12	83	17
Control-7d	88	12	91	9	93	7
***A.f*+Realgar+0 g ZVI-1d**	79	21	85	15	82	18
***A.f*+Realgar+0 g ZVI-7d**	50	50	11	89	12	88
***A.f*+Realgar+0.2 g ZVI-1d**	83	18	8	15	89	11
***A.f*+Realgar+0.2 g ZVI-7d**	2	98	24	76	32	68
***A.f*+Realgar+2.0 g ZVI-1d**	33	67	75	25	82	18
***A.f*+Realgar+2.0 g ZVI-7d**	18	82	63	37	63	37

1.8 The As-Fe-O-H-S system for the experiments

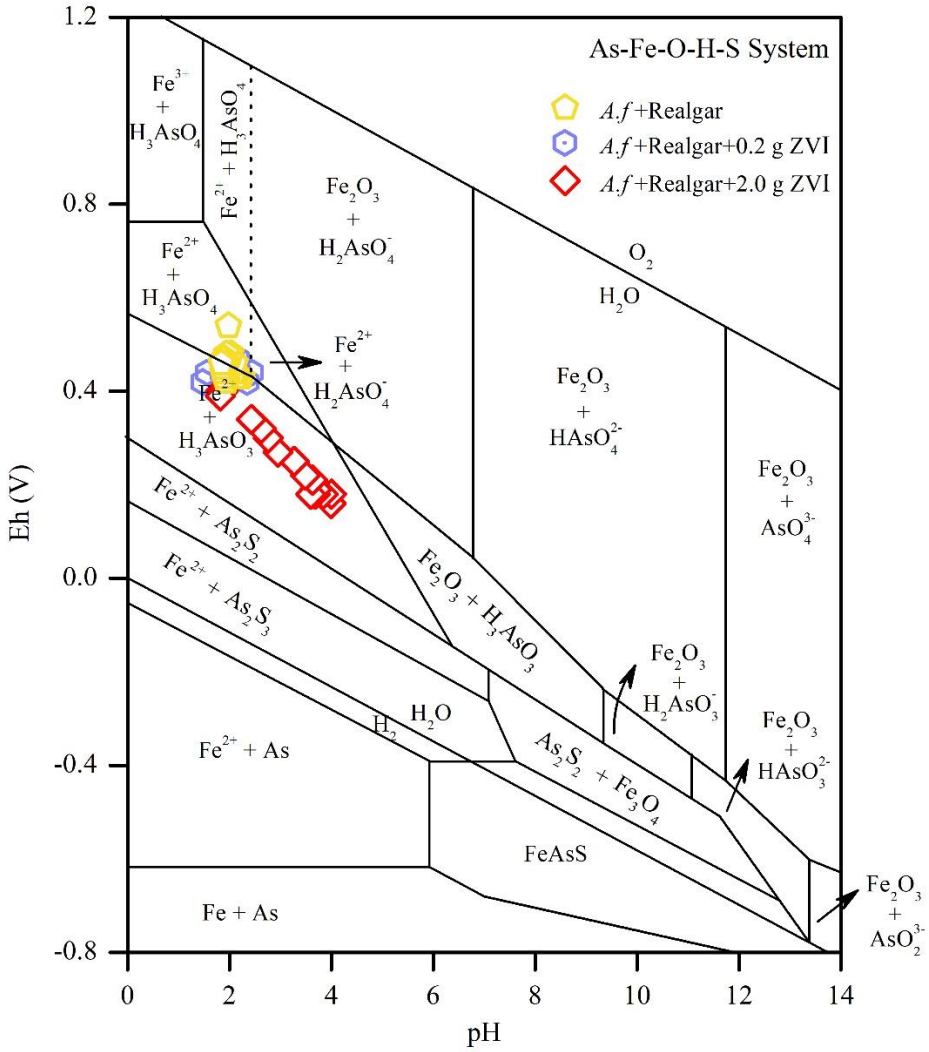

Fig. S6 Eh-pH diagram for the system As-Fe-O-H-S
at 25 °C and 1.013 bars total pressure. $\sum\{Fe\} = \sum\{S\} = \sum\{As\} = 10^{-6}$.

The As-Fe-O-H-S phase diagram (Fig. S6) shows which phases were to be expected at metastable equilibrium under acidic to circumneutral pH conditions. In the 2.0 g ZVI-added experiment As(III) was the dominant phase, and in the 0.2 g and 0 g ZVI-added treatments As(III) and As(V) both existed. These data suggested that mixed As-Fe oxyhydroxides and oxyhydroxy sulfates formed during the experiments.